Reduction of Secondary Flow Effects in a Linear Cascade by Use of an Air Suction from the Endwall

K. Funazaki and T. Endo
Department of Mechanical Engineering
Iwate University
Morioka, Japan

T. Tanuma
Heavy Apparatus Engineering Laboratory
Toshiba Corporation
Yokohama, Japan

ABSTRACT

The objective of this study is to reduce secondary flow effects in a linear cascade by sucking the working fluid from the endwall. It is widely known that the secondary flow developed in a cascade has a significant impact on the cascade loss or blade erosion in steam turbines. Therefore, a number of studies have been made on the physics of the secondary flow and several devices to control the secondary flow, such as a fence, have been examined. In this study, considering the application to nozzles in gas turbines or steam turbines, the air suction approach is investigated for reducing the secondary flow effects. The effects of the suction upon the flow nearby the endwall and the secondary flow are confirmed by several flow visualizing techniques, for example an oil flow method or a tuft method. The flow rate of the sucked air is controlled by adjusting the back pressure in the plenum chamber. Furthermore, velocity and total pressure are measured using a hot-wire anemometer and a five-hole pressure tube, which provides the velocity and total pressure profiles within the flow passage after the suction slot.

NOMENCLATURE

C_x	: axial chord length
H	: blade span
h_0	: stagnation enthalpy
P	: suction pressure ratio
p_{chamber}	: pressure in the suction chamber
p_{slit}	: pressure at the slit
P_0	: total pressure
$\dot{q}, \dot{q}_c$	: main flow rate, sucked flow rate
Re	: Reynolds number (= $V_1 C_x / \nu$)
T	: blade pitch
V_1	: inlet velocity
x, y, z	: axial, tangential and spanwise coordinates
ρ	: density
ν	: kinematic viscosity
ω	: vorticity
ζ	: total pressure loss coefficient
subscript	
0	: stagnation condition
1, 2	: inlet, outlet
a	: ambient condition
mid	: midspan
superscript	
$\bar{}$	: pitchwisely mass-averaged quantity
$\tilde{}$	: mass-flow averaged quantity over the traverse plane

INTRODUCTION

It is widely recognized that secondary flows occurring in a stator and a rotor is a major source of loss generation in turbomachines. Especially, endwall loss, which can be attributed to a passage vortex originating from a horseshoe vortex, reportedly contributes almost one-third of the total loss of a cascade (Denton, 1993). We hereafter refer to the passage vortex and its associated vortical motion of fluid as secondary flow for simplicity.

Apart from the aerodynamic aspect, the secondary flow is important in the structural problems in steam turbines. Funazaki et al. (1993) pointed out that water droplets deposited on the endwall of the last-stage stator were significantly influenced by the secondary flow (passage vortex) so that the droplets drifted towards the suction side of the stator blade and were convected along the blade surface. This resulted in an increase in the number of water droplets leaving the trailing edge of the stator blade, which would make a great contribution to erosion of the subsequent rotor blades by hitting the blade surfaces.

A number of studies have been made on the secondary flow for decades, for example Langston et al. (1977). A comprehensive review on secondary flows in turbine cascades is provided by Sieverding 1985). More recently, Wang et al. (1995) made a detailed flow visualization of the secondary flow by use of a smoke wire method, and proposed a secondary flow model in a cascade as shown in Fig. 1. However, It does not seem that thorough understanding of the secondary flow is within our reach because of its complicated structure.

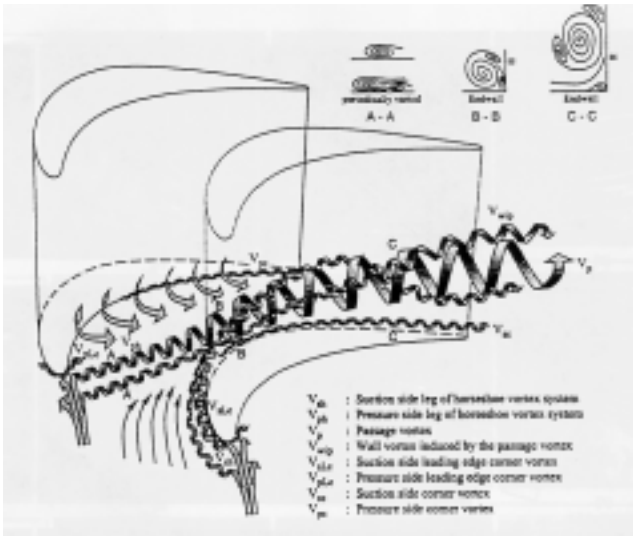

Fig. 1 Secondary flow model in a turbine cascade (Wang et al., 1995)

Moreover, there are a number of factors that could influence the secondary flow but are not sufficiently examined, such as blade stacking, flare angle of the passage, load distribution, skewed inlet boundary layer and Reynolds number. Despite this difficult situation, designers of compressor or turbine blades have been devoting their efforts to the reduction of the endwall loss by optimization of the spanwise loading distribution or by applying leaned or bowed stacking of the blade sections. In addition, endwall fences or blade fences have also been examined as a device to achieve a meaningful suppression of the endwall loss, for example by Kawai et al. (1994) and Funazaki et al. (1994). Funazaki et al. found that blade surface fences could suppress the endwall loss, however the presence of the fence caused additional loss.

In this study, taking account of the application to nozzles in gas turbines or steam turbines, the present study was conducted to investigate the validity of the air suction method from the endwall of a cascade for decreasing the endwall loss and for reducing the generation of erosive water droplets in a steam turbine case.

TEST APPARATUS

Model cascade

Figure 2 shows a schematic layout of the test apparatus used in this study. The test cascade, as shown in Fig. 3, is a linear cascade composed of five acrylic-resin blades. Some of the blades are coated with black paint for flow visualization. The blade section is based on a typical last-stage stator blade section for steam turbines and its scale is almost the same as that of the actual units. The blade pitch T is 200 mm, the blade span H is 150 mm and the axial chord length C_x is 250 mm; the aspect ratio of the blade is accordingly 0.67. Each blade is fixed to the upper and lower acrylic plates and silicon sealant is pasted on both ends of the blade to avoid any air-leakage from the pressure side to the suction side. The front ends of those upper and lower plates are sharp-edged. There are 10-mm spacings between the transition duct and the plates, discharging some amount of the flow through those spacings to refresh a boundary layer from the edge. Eight slots are provided in the upper acrylic plate for the aerodynamic measurement by use of a five-hole Pitot tube.

The water supply system for simulating water deposition onto the casing of a steam turbine is schematically shown in Fig. 4. Water

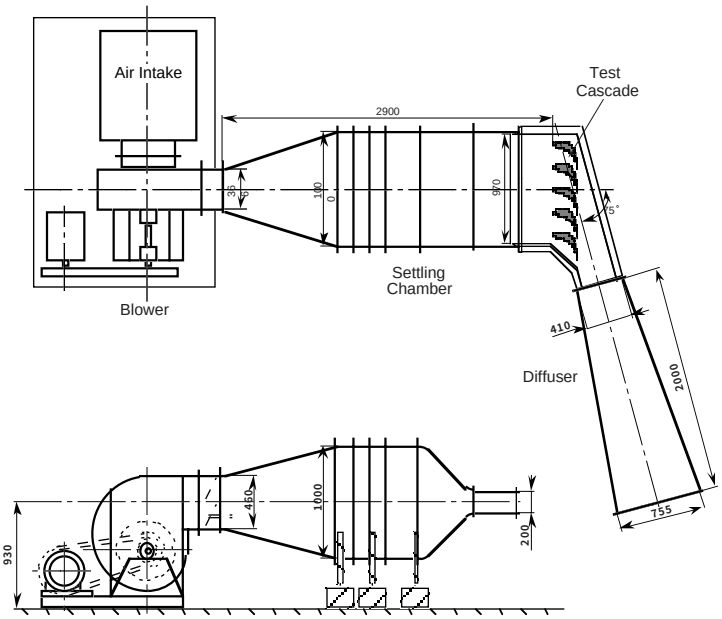

Fig. 2 Schematic layout of the test apparatus

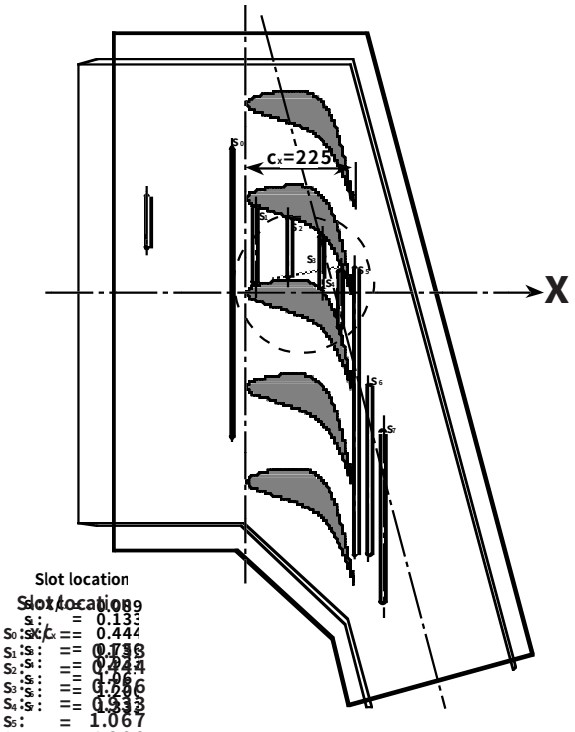

Fig. 3 Top view of the test cascade with the location of the measurement slots and suction slit

from an overhead tank is distributed equally to seven feeding holes 2 mm in diameter located 80 mm upstream from the blade leading edge. The flow rate of the fed water is measured with a miniature laminar-flowmeter. A controller automatically keeps the water

Table 1 Geometrical data and flow conditions

	Actual Unit	Test Model
Axial Chord [m]	0.225	0.225
Pitch [m]	0.200	0.200
Span [m]	-	0.15
Inlet Total Pressure [MPa]	0.137	0.098
Inlet Total Temperature	75	20
Inlet Flow Angle [deg]	0	0
Outlet Flow Angle [deg]	75	75
Kinematic Viscosity [m²/s]	5.5×10^{-5}	1.5×10^{-5}
Reynolds Number	1.3×10^{6}	0.66×10^{6}
Exit Mach Number	0.8	0.15
Working Fluid	Sat.Steam	Dry Air

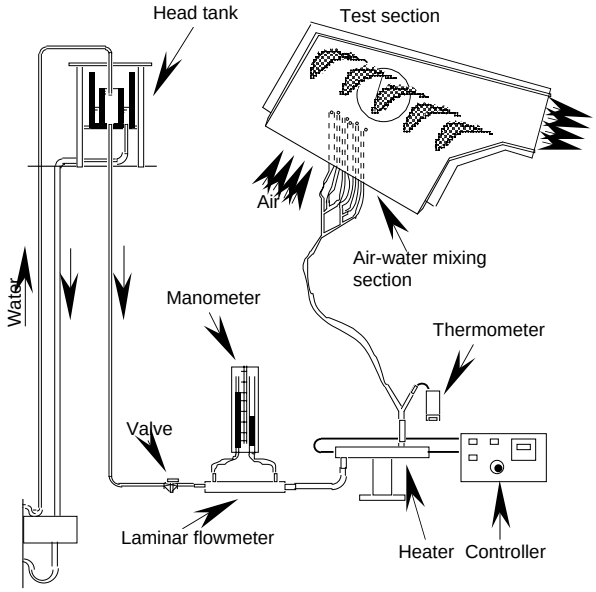

Fig. 4 Water supply system for simulation of water deposition on the outer casing of a steam turbine

temperature almost constant ($\approx 20°C$) throughout a test run. Funazaki et al. (1994) found in the previous study that the motion of the water deposited on the endwall was significantly influenced by the secondary flow so that the water on the endwall climbed onto the blade suction surface. They also showed that the controlled secondary flow by use of a blade fence, for example, changed the water motion drastically. Therefore, observations of the water motion helps us understand to what extent the air-suction affects the secondary flow.

An air suction slit of 1 mm in width and 140 mm in length is provided between the pressure side of blade #2 and the suction side of blade #3 in the lower plate, as shown in Fig. 3. A three-dimensional

Table 2 Suction pressure ratios and sucked flow rate

	P	qc / q [%]
case 1	0.971	0.7
case 2	0.933	2.5
case 3	0.743	6.6

Navier-Stokes solver was employed to calculate the flow field (Ono, 1995), which determined the position of the suction slit so that the slit was situated almost along an iso-pressure line on the endwall. The slot is inclined by 45 deg from the lower plate surface. A plenum chamber is attached to the back side of the lower plate and it is connected to a vacuum pump. The flow rate of the sucked air, controlled by adjusting the back pressure in the plenum chamber, is measured with a laminar-flowmeter (Sokken, LFE-50B). All equipment, including a valve and a tank for measuring the quantity of the sucked water, are connected through thick rubber tubes. Table 1 shows suction pressure ratios P adopted and the corresponding mass flow rates $\dot{q}_c$ with respect to the main flow rate for one blade-to-blade passage $\dot{q}$, where P is defined as

$$P = p_{\text{chamber}} / p_{\text{slit}} \ , \qquad (1)$$

where p_{chamber} is the pressure inside the plenum chamber and p_{slit} is the averaged pressure along the inlet of the suction slit.

Table 1 shows the summary of the geometrical data and the flow conditions of the model cascade in comparison with those of an actual unit. Even though the Reynolds number was almost halved for the test case, we believe the present test facility provides a sufficient environment to simulate the actual flow situation.

Instruments

Aerodynamic measurements were carried out mainly using a pneumatic five-hole probe in this study. This probe has a considerably large opening above the sensing head so that the blockage effect of the probe is minimal. Calibration of the probe was made with great care at a calibration wind tunnel, and calibration curves for yaw angle, pitch angle and total pressure were determined. A detailed description on the probe itself and the probe calibration process was reported by Matsubara (1993). The probe is maneuvered by a computer-controlled 3-axial traverse unit in each slot, while inlet velocity and total pressure are being monitored by a standard L-type Pitot tube. A single hot-wire probe with a CTA (Constant Temperature Anemometer), Kanomax system 7201, determines the inlet boundary layer thickness. Pressure transducers (Kyowa PDL-40GB, rated range $\pm$ 3.9 kPa) detect the pressures, and the measured signals were sampled by a computer-controlled datalogger (NEC San-ei, 7V14). The method of Klein and McClintock (1953) revealed that uncertainty contained in the pressure value was about $\pm$ 4.9 Pa (95% coverage).

DATA PROCESSING

Total Pressure

Total pressure loss coefficient is defined as

$$\zeta(y,z) = \frac{P_{0,1} - P_0(y,z)}{\frac{1}{2}\rho V_1^2} \ , \qquad (2)$$

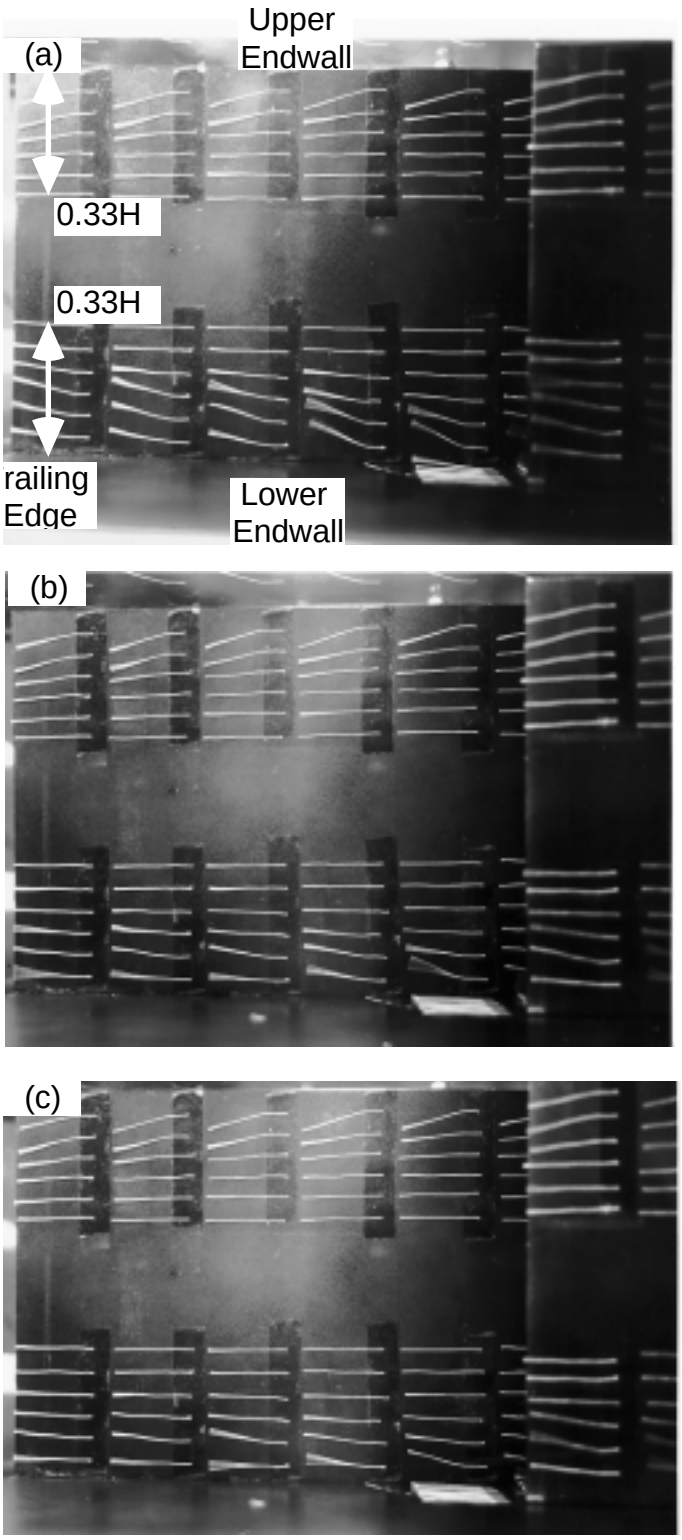

Fig. 5 Behaviors of tufts on the blade suction surface (a) P=1 (no suction) (b) P=0.933 (c) P=0.733

upstream of the cascade, $P_0(y,z)$ is the total pressure measured by the five-hole pressure tube and $1/2\rho V_1^2$ is an inlet dynamic pressure.

Vorticity

Conventionally, the vorticity associated with the secondary flow is defined as the one having its axis along the primary flow direction

(θ_{mid}) and is calculated as follows;

$$\omega_s = \omega_x \cos\theta_{mid} + \omega_y \sin\theta_{mid} \tag{3}$$

where ω_x and ω_y are axial and tangential vorticity components, respectively, and the flow at the midspan is considered to represent the primary flow with the flow angle θ_{mid}. Calculation of Eq. (3) requires the tangential vorticity ω_y, but it is not easy to calculate the vorticity accurately because of the relatively large axial spacings between the traverse slots. Therefore, for the purpose of depicting the secondary flow structure, we use the axial vorticity contours instead. This provides us a view of a vortex on a y-z plane cutting the vortex obliquely to its axis, from which one can obtain an image of the vortex that is a little wider than the actual one. Note that a velocity and a length are normalized by the inlet velocity V_1 and the axial chord length C_x, which means the vorticity is normalized by V_1/C_x.

FLOW VISUALIZATION

Tuft Method

We equipped a number of thin and light tufts of 30 mm in length on the endwall as well as the blade suction surface to visualize the flow field over there in a real-time mode. Those tufts were attached to the surface with adhesive tape. In this case, much attention was paid to the flexibility of the tufts. Figure 5 shows the photographs of the tuft behavior on the blade suction surface near the trailing edge with and without the endwall suction. These pictures clearly demonstrate the effect of the endwall suction upon the secondary flow. In the case of no-suction from the slit, as shown in Fig. 5 (a), the tails of those tufts move towards the blade center line due to the passage vortex developed near the suction surface. Furthermore, the tufts near the lift-off line or separation line, which was observed by oil flow pattern, flutter forcefully. As the sucked flow rate increased, the tufts over the lower portion of the blade tended to be aligned in parallel to the endwall, as seen in Figs. 5 (b) and 5 (c). It can be concluded from these observations that the endwall suction affected the passage vortex so effectively that the spanwise velocity component over the suction surface, which was associated with the passage vortex, was significantly reduced. As described later, this effect seems to be beneficial to desingers of steam turbines from the viewpoint of minimizing the possibility of rotor blade erosion caused by water droplets from the stator blade surface.

Water Movement

Figure 6 displays photographs of the water behavior on the lower endwall with and without suction from the suction slit. The flow rate of the fed water from the injection ports was 0.200 m^3/min for this case. This flow rate, which is probably larger than could be expected in an actual situation, was rather arbitrarily chosen because there are little information about it. Figure 7 shows the water recovery ratio of the suction slit for several suction pressures in the tank attached to the lower plate, which is defined as

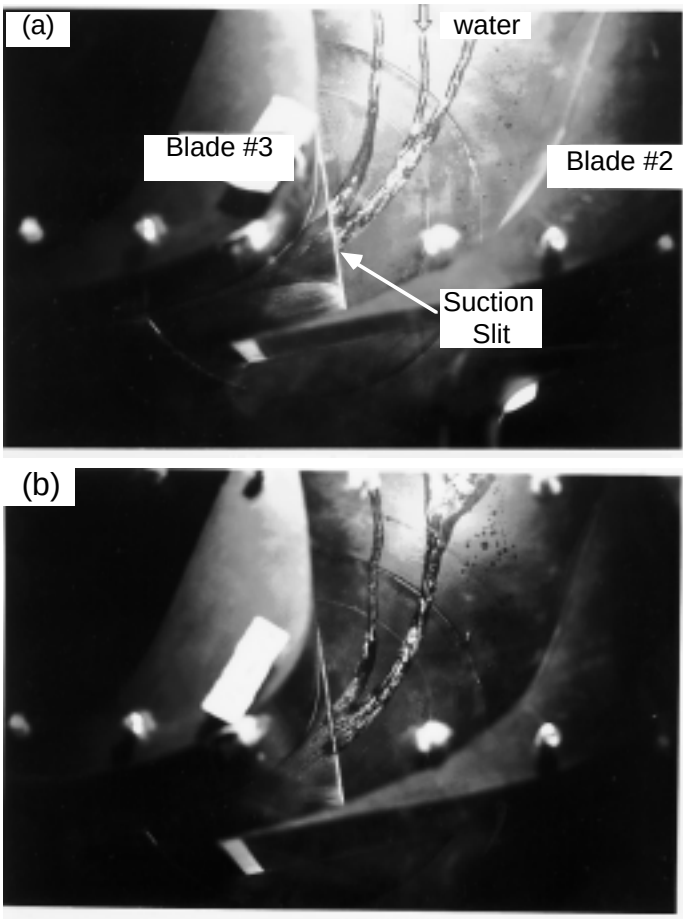

Fig. 6 Behaviors of water deposited on the lower endwall (a) P=1 (no suction) (b) P=0.933

$$\text{Recovery ratio} = \frac{\text{Water volume captured during 20 minutes}}{\text{Water volume supplied during 20 minutes}}.$$

In the case of no-suction (Fig. 6 (a)), the water fed at the upstream of the cascade moved downward and gradually flattened due to the flow acceleration. Most of the water went over the suction slit, however, a small amount of the water was trapped by the slit even without suction. Passing across the slit, the water drifted towards the blade suction surface, then climbed the suction surface due to the action of the passage vortex. The water consequently moved to the blade trailing edge and was shed downwards in the form of water droplet. When the suction started, the water tended to be sucked into the slit. As seen in Fig. 6 (b) or Fig. 7 most of the water was captured by suction slit for the suction pressure ratio less than 0.95 and no water was rolled up onto the blade suction surface, which was in contrast with the observation for the no-suction case. These phenomena can be explained from two features of the suction slit; one is to eliminate the water on the endwall by suction and the other is to weaken the effect of the passage vortex on the upward movement of the flow over the suction surface, as confirmed by the tuft method. It can be, therefore, concluded that the suction slit on the endwall is useful for controlling the secondary flow, i.e., the passage vortex developed in the blade-to-blade passage, furthermore the suction slit is quite beneficial to steam turbines because it works to reduce the

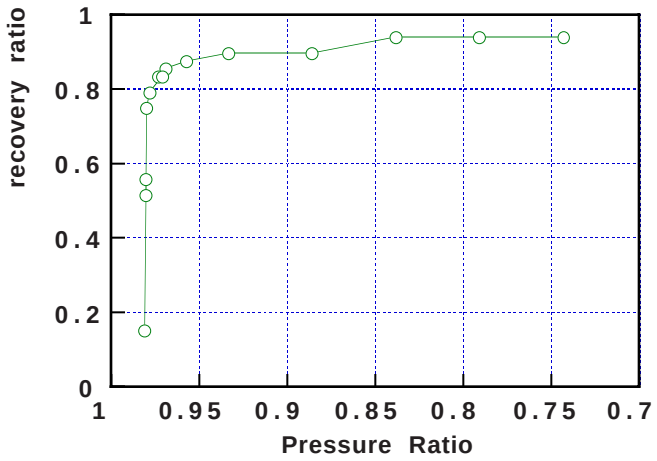

Fig. 7 Water recovery ratio of the suction slit

the rear rotor blades.

AERODYNAMIC MEASUREMENTS

Inlet Boundary Layer

The inlet boundary layer is measured at slot 0 ($x/C_x = -0.089$) by a single hot-wire probe, where the tangential location of this measurement was at the center of the blade-to-blade passage. This measurement revealed that the inlet boundary layer was almost turbulent and its thickness was about 3 mm.

Measurements at the cascade exit

Figure 8 shows the distributions of total pressure loss coefficient and secondary vorticity measured at slot #6 in the case of no suction from the endwall. For convenience, the abscissa and the ordinate of each of the diagrams are normalized by the blade pitch P and by the blade span H, respectively. In these figures, $y/T = 0$ represents the crossing line of the plane extended streamwisely from the trailing edge of blade #3 with the traverse plane of slot #6, and $z/H = 0$ corresponds to the midspan line. Note that the measurements were conducted over the lower half of the traverse plane, assuming symmetry with respect to the midspan line. In fact, preliminary studies done by Endo (1996) revealed that the endwall suction slightly deteriorated the flow symmetry. However, the observed variation in the flow pattern was almost comparable to the pitchwise variation in the cascade even for the maximum suction case in this study. This accordingly implies that the following discussion on the effect of the endwall suction does not lose the generality.

Total pressure loss distribution in the upper diagram of Fig. 8 is a typical one for the flow field downstream of turbine cascades. A peak of the total pressure loss or a loss core, which could be divided into two parts, appears around $z/H \cong -0.25$. The lower diagram of Fig. 8 clearly displays a complicated vortical flow field of the cascade exit. Note that an area with positive value of the vorticity represents a counter clockwise vortical motion and vice versa for an area with negative vorticity. One can conclude that the area with negative vorticity denoted as PV corresponds to a passage vortex. However, as for the area with positive vorticity denoted as CV, different conclusions have been drawn by several researchers. For example, Goldstein and Spores (1988) stated it was the suction side horseshoe leg that moved with the passage vortex. On the other hand, Sharma and Butler (1987)

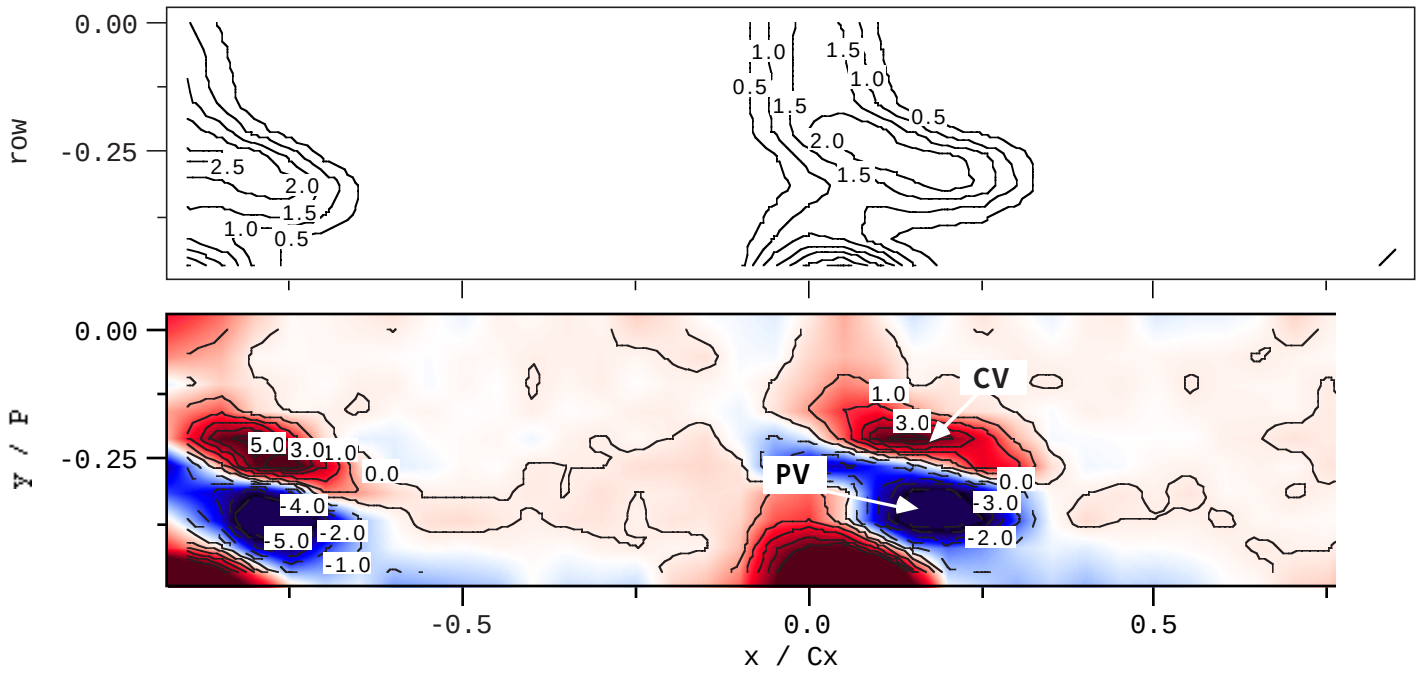

Fig. 8 Measurements of total loss and secondary vorticity distributions for the no-suction case at the slot #6 (upper) Total loss (lower) Secondary Vorticity

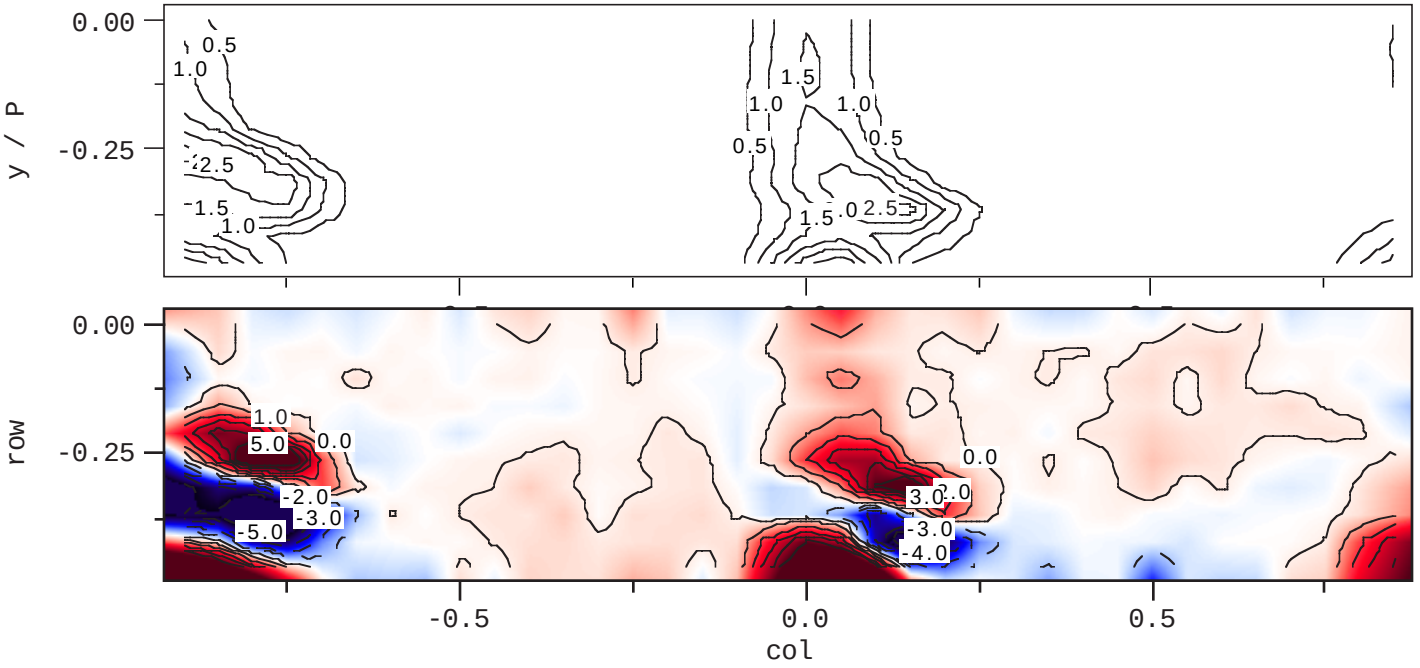

Fig. 9 Measurements of total loss and secondary vorticity distributions for medium suction case (P=0.933) at the slot #6 (upper) Total loss (lower) Secondary Vorticity

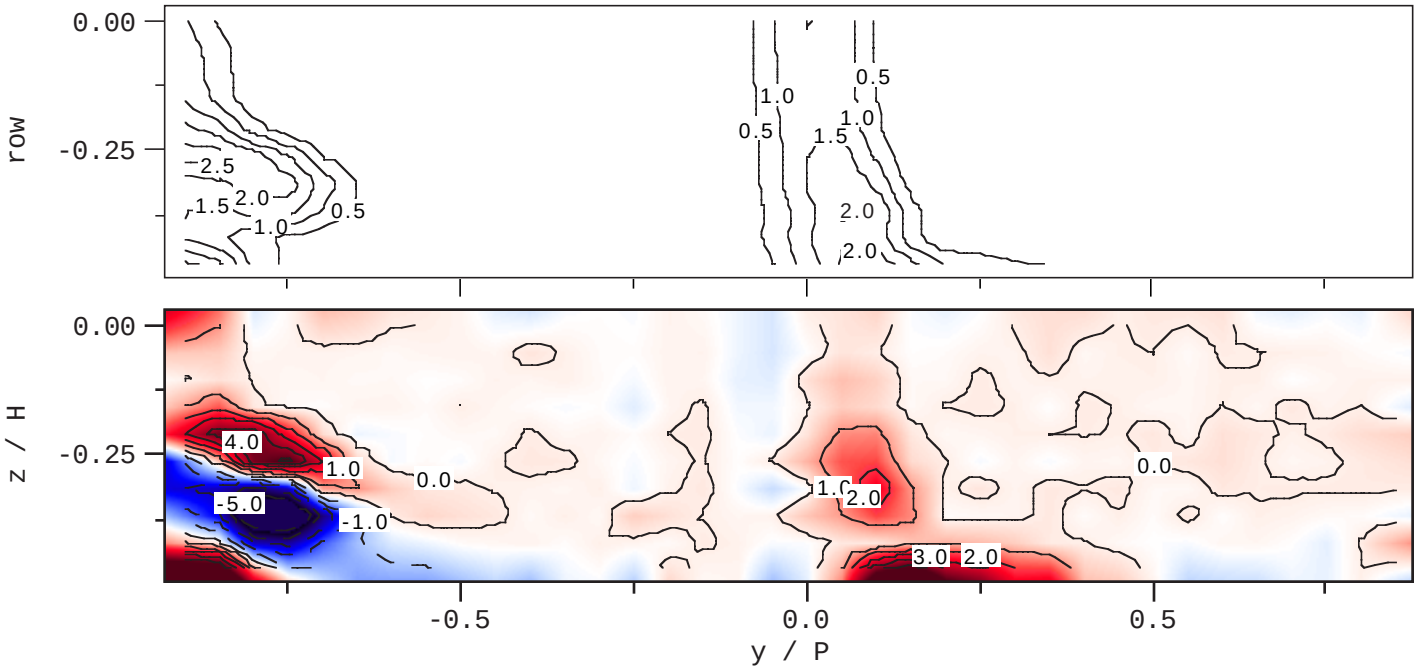

Fig. 10 Measurements of total loss and secondary vo
(upper) Total los

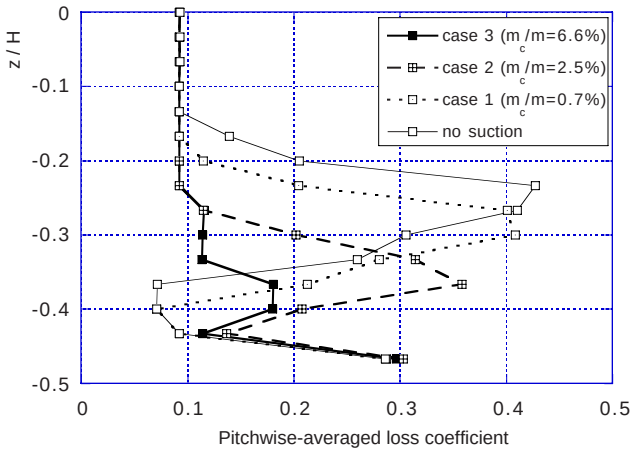

Fig. 11 Pitchwisely mass-averaged loss coefficient

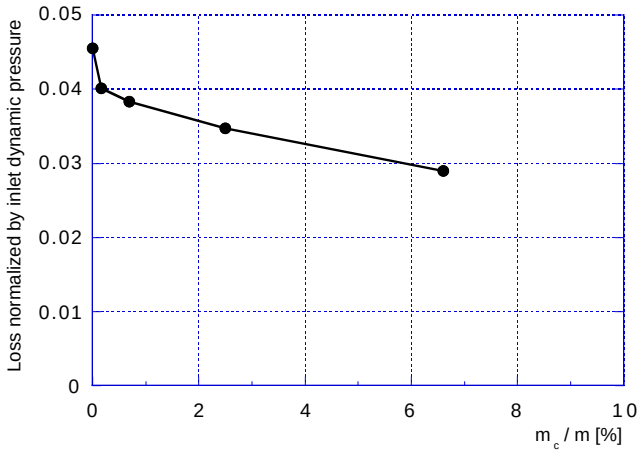

Fig. 12 Loss reduction by the endwall suction

a wall vortex, mentioning that it was induced by the passage vortex (See Fig. 1). Because it is beyond the scope of the present paper to discuss further on this point, we simply refer to it as counter vortex.

When the endwall suction initiates, as seen in Fig. 10, the loss core and vortex cores descend towards the endwall and they decrease significantly. Figure 10 shows that the loss and vorticity cores almost diminish for the most intense suction case among the present experiments, and only a small area with negative vorticity remains discernible. This is seemingly a trailing vortex from blade #3.

Figure 11 shows spanwise distributions of pitchwisely mass-averaged loss coefficient $\bar{\xi}$, which is defined by

$$\bar{\xi}(z) = \frac{1}{\frac{1}{2}\rho V_1^2} \frac{\int_{slot\#6} \rho\left(P_{01} - P_{02}(y,z)\right) V(y,z)\,dy}{\int_{slot\#6} \rho V(y,z)\,dy}, \qquad (4)$$

for several suction mass flow rates. As seen in the above, the position of the averaged loss peak descends from $z/H \cong -0.23$ to $z/H \cong -0.4$ with the increase in suction mass flow rate. The peak value of the loss decreases due to the suction from 0.42 to 0.18. One may notice that the loss distribution exhibits little spanwise variation in the maximum suction case, which gives us an impression that the passage vortex almost vanishes. Figure 12 shows the effect of the endwall suction on the mass-averaged loss coefficient over the measured area. The

averaged loss decreases by 36% for the maximum suction, which is a significant improvement on the turbine performance.

DISCUSSION

When applying the endwall suction to an actual steam turbine, effects of sucked air upon the overall efficiency of a turbine must be considered, although a rigorous estimation on such effects is not a simple task to execute. Since the inlet boundary layer thickness was 3 mm, an estimation yielded that its displacement thickness was about 1 mm, implying that the ratio of the displaced flow rate to the mainstream flow rate was about 0.7%. Assuming that

CONCLUSIONS

The experiments were conducted to examine the effects of the air-suction from the endwall on the aerodynamic performance of the test cascade as well as on the water movement over the endwall and blade surfaces. The results are itemized as follows:

(1) Flow visualization by a tuft method revealed that the endwall suction suppressed the evolution of the passage vortex.

(2) Large amount of the water deposited on the endwall is captured by the suction slit even for a moderate suction pressure case.

(3) The endwall suction successfully controlled the passage vortex developed within the blade-to-blade passage, resulting in significant reduction of the cascade loss.

ACKNOWLEDGMENT

The authors are greatly indebted to Mr. H. Ogawa for his contribution in conducting the experiments.

REFERENCES

Denton, J. D., 1993, "Loss Mechanisms in Turbomachines," Trans. ASME *Journal of Turbomachinery*, Vol. 115, pp. 621 - 656.

Endo, T., 1996, "Studies on Controlling Secondary Flows Developed in Steam Turbines," Master Thesis, Iwate University.

Funazaki, K., Matsubara, H., Nakano, S., Tanuma, T. and Nagao, S., 1993, "Secondary Flow Effect on Water Movement over the Surfaces of a Steam Turbine Cascade," Proc. JSME-ASME International Conference on Power Engineering - 93 (ICOPE-93), Vol. 2, pp. 355 - 360.

Funazaki, K., Nakano, S. and Tanuma, T., 1994, "Secondary Flow Effects on Water Movement in a Steam Turbine Cascade (Reduction of the Secondary Flow Effect by Endwall and Blade Fences)," Proc. 3rd JSME-KSME Fluid Engineering Conference, pp. 686 - 691.

Goldstein, R.J. and Spores, R.A., “Turbulent Transport on the Endwall in the Region between Adjacent Turbine Blades,” Trans. ASME *Journal of Heat Transfer*, Vol.110, pp. 862-869.

Kawai, T., Ohshige, H., Nakai, K. and Adachi, T., 1994, "Effect of Boundary Layer Fences Attached to Casing of Annular Turbine Nozzle Cascade (in Japanese)," *JSME Transaction, B series*, Vol. 60, pp. 169 - 175.

Kline, S. J. and McClintock, F. A., 1953, "Describing Uncertainties in Single Sample Experiments," *Mechanical Engineering*, Vol. 75 pp. 3 - 8.

Langston, L. S., Nice, M. L. and Hooper, R. M., 1977, "Three Dimensional Flow Within a Turbine Blade Passage," Trans. ASME *Journal of Engineering for Power*, Vol. 99, pp. 21-28.

Matsubara, H., 1993, "Secondary Flows in a Model Cascade of a Steam Turbine," Master Thesis, Iwate University

Ono, K., 1995, "Three-Dimensional Navier-Stokes Flow Analyses around the Stator Cascade of a Steam Turbine," Bachelor Thesis, Iwate University

Sharma, O. P. and Butler, T. L., 1987, "Predictions of Endwall Losses and Secondary Flows in Axial Flow Turbines Cascades," Trans. ASME *Journal of Turbomachinery*, Vol. 109, pp. 229-236.

Sieverding, C. H., 1985, "Recent Progress in the understanding of Basic Aspects of Secondary Flows in Turbine Blade Passages," Trans. ASME *Journal of Engineering for Das Turbines and Power*, Vol. 107, pp. 248-257.

Wang, H. P., Olson, S. J., Goldstein, R. J. and Eckert, E. R. G., 1995, "Flow Visualization in a Linear Turbine Cascade of High Performace Turbine Blades," ASME Paper 95-GT-7.